

Equation of state and thickness of the inner crust of neutron stars

Fabrizio Grill, Helena Pais, Constança Providência, and Isaac Vidaña
*Centro de Física Computacional, Department of Physics,
University of Coimbra, P-3004-516 Coimbra, Portugal*

Sidney S. Avancini

Depto de Física - CFM - Universidade Federal de Santa Catarina Florianópolis - SC - CP. 476 - CEP 88.040 - 900 - Brazil

The cell structure of β -stable clusters in the inner crust of cold and warm neutron stars is studied within the Thomas–Fermi approach using relativistic mean field nuclear models. The relative size of the inner crust and the pasta phase of neutron stars is calculated, and the effect of the symmetry energy slope parameter, L , on the profile of the neutron star crust is discussed. It is shown that while the size of the total crust is mainly determined by the incompressibility modulus, the relative size of the inner crust depends on L . It is found that the inner crust represents a larger fraction of the total crust for smaller values of L . Finally, it is shown that at finite temperature the pasta phase in β -equilibrium matter essentially melts above 5–6 MeV, and that the onset density of the rodlike and slablike structures does not depend on the temperature.

PACS number(s): 21.65.Cd, 24.10.Jv, 26.60.-c, 97.60.Jd

I. INTRODUCTION

Nowadays, it is generally accepted the existence of the so-called *pasta phase* [1–10] in the inner crust of a neutron star close to the crust-core transition. Constituted by several types of complex structures such as *e.g.*, rods and slabs, the pasta phase is a frustrated system formed as a result of the competition between the strong and the electromagnetic interactions.

The effect of the density dependence of the symmetry energy on the pasta phase has been discussed in several works [11–14]. In particular, it has been shown that for very large values of the symmetry energy slope parameter, $L = 3n_0(\partial E_{sym}(n)/\partial n)_{n_0}$, non-spherical structures (*e.g.*, rodlike or slablike) are not expected in β -equilibrium matter, and that the number of nucleons in the clusters as well as the cluster proton fraction and the size of the Wigner–Seitz (WS) cell are sensitive to this quantity. It has been also discussed that L may have quite dramatic effects on the cell structure if its value is very large or small [9, 12, 13].

In the present work the effect of L on the size of the inner crust will be discussed within a Thomas–Fermi (TF) formalism in the WS approximation in the framework of relativistic mean-field (RMF) nuclear models [6–9]. The Tolman–Oppenheimer–Volkov equations (TOV) [15] will be integrated and the size of the inner crust as well as the localization of the pasta structures identified. In particular, it will be shown that smaller values of L favor a wider slab phase and a larger relative size of the inner crust with respect to the total crust, and a steeper crust profile.

We will also study the effect of temperature on the size of the inner crust. It will be shown that pasta clusters

in β -equilibrium will completely melt for temperatures above 5-6 MeV. These results agree partially with the predictions obtained within a dynamical spinodal (DS) approach [16–18]. A similar calculation was done with Skyrme forces in Ref. [19]. The melting of the pasta phase was previously studied in [20, 21], where the effect of thermal fluctuations was taken into account. It is expected that if thermal fluctuations are larger than the radius of the WS cell, the WS approximation breaks down. However, thermal fluctuations will not be considered in the present calculation and, therefore, the reader must interpret our results just as upper limits. The existence of non-homogeneous matter will affect the evolution of a supernova or proto-neutron star matter, in particular the diffusion of neutrinos out of the star [3]. Some preliminary results of the present study have been published in Ref. [14].

The paper is organized as follows. The formalism is briefly reviewed in section II. Section III is devoted to the presentation and discussion of the results while the main conclusions are given in section IV.

II. FORMALISM

To describe the inner crust in this work we apply the self-consistent TF formalism presented in Refs. [7–9]. We use relativistic mean field nuclear models with constant couplings and non-linear terms [22], and with density dependent couplings [23]. Within the first class of models, that we will designate by Non Linear Walecka Models, we consider the following ones: NL3 [24] with non linear σ terms, TM1 [25] with non linear σ and ω terms, NL3 $_{\omega\rho}$ including also non-linear $\omega\rho$ terms which allow the modulation of the density dependence of the symmetry energy [26], FSU [27] and IU-FSU [28] with non-linear σ , ω and $\omega\rho$ terms. Within the second class of models with density dependent couplings we consider the models DD-ME2 [29] and DD-ME δ [30]. The latter, among the

parametrizations considered, is the only one including the δ meson.

All the equations that allow the performance of the TF calculation are derived from the Lagrangian density

$$\mathcal{L} = \sum_{i=n,p} \mathcal{L}_i + \mathcal{L}_e + \mathcal{L}_\sigma + \mathcal{L}_\omega + \mathcal{L}_\rho + \mathcal{L}_\delta + \mathcal{L}_\gamma + \mathcal{L}_{nl}, \quad (1)$$

where the nucleon Lagrangian reads

$$\mathcal{L}_i = \bar{\psi}_i [\gamma_\mu i D^\mu - M^*] \psi_i, \quad (2)$$

with

$$i D^\mu = i \partial^\mu - \Gamma_\omega \omega^\mu - \frac{\Gamma_\rho}{2} \boldsymbol{\tau} \cdot \boldsymbol{\rho}^\mu - e \frac{1 + \tau_3}{2} A^\mu, \quad (3)$$

$$M^* = M - \Gamma_\sigma \sigma - \Gamma_\delta \boldsymbol{\tau} \cdot \boldsymbol{\delta}, \quad (4)$$

and the electron Lagrangian is given by

$$\mathcal{L}_e = \bar{\psi}_e [\gamma_\mu (i \partial^\mu + e A^\mu) - m_e] \psi_e. \quad (5)$$

The meson and electromagnetic Lagrangian densities are

$$\begin{aligned} \mathcal{L}_\sigma &= \frac{1}{2} (\partial_\mu \sigma \partial^\mu \sigma - m_\sigma^2 \sigma^2) \\ \mathcal{L}_\omega &= \frac{1}{2} \left(-\frac{1}{2} \Omega_{\mu\nu} \Omega^{\mu\nu} + m_\omega^2 \omega_\mu \omega^\mu \right) \\ \mathcal{L}_\rho &= \frac{1}{2} \left(-\frac{1}{2} \mathbf{R}_{\mu\nu} \cdot \mathbf{R}^{\mu\nu} + m_\rho^2 \boldsymbol{\rho}_\mu \cdot \boldsymbol{\rho}^\mu \right) \\ \mathcal{L}_\delta &= \frac{1}{2} (\partial_\mu \boldsymbol{\delta} \partial^\mu \boldsymbol{\delta} - m_\delta^2 \boldsymbol{\delta}^2) \\ \mathcal{L}_\gamma &= -\frac{1}{4} F_{\mu\nu} F^{\mu\nu} \\ \mathcal{L}_{nl} &= -\frac{1}{3!} \kappa \sigma^3 - \frac{1}{4!} \lambda \sigma^4 + \frac{1}{4!} \xi \Gamma_\omega^4 (\omega_\mu \omega^\mu)^2 \\ &\quad + \Lambda_\omega \Gamma_\omega^2 \Gamma_\rho^2 \omega_\nu \omega^\nu \boldsymbol{\rho}_\mu \cdot \boldsymbol{\rho}^\mu \end{aligned}$$

where $\Omega_{\mu\nu} = \partial_\mu \omega_\nu - \partial_\nu \omega_\mu$, $\mathbf{R}_{\mu\nu} = \partial_\mu \boldsymbol{\rho}_\nu - \partial_\nu \boldsymbol{\rho}_\mu - \Gamma_\rho (\boldsymbol{\rho}_\mu \times \boldsymbol{\rho}_\nu)$ and $F_{\mu\nu} = \partial_\mu A_\nu - \partial_\nu A_\mu$. The four coupling parameters Γ_σ , Γ_ω , Γ_ρ and Γ_δ of the mesons to the nucleons are density dependent in the relativistic density dependent models considered, namely, DD-ME2 [29] and DD-ME δ [30]. The non-linear term \mathcal{L}_{nl} is absent in these models. In all the other models, NL3 [24], TM1 [25], NL3 $_{\omega\rho}$ [26], FSU [27] and IU-FSU [28], the couplings are constant and at least some of the non-linear terms of \mathcal{L}_{nl} are included. In the above Lagrangian density $\boldsymbol{\tau}$ is the isospin operator. For reference, we give in Table I the main properties of the above models at saturation density. We will discuss how sensitive is the structure of the non-homogeneous inner-crust of a neutron star to the properties of the Equation of State (EoS).

In the TF approximation of non-uniform npe matter, fields are assumed to vary slowly so that baryons can be treated as moving in locally constant fields at each point [6, 7]. The calculation starts from the grand canonical potential density,

$$\begin{aligned} \omega &= \omega(\{f_{i+}\}, \{f_{i-}\}, \sigma, \omega_0, \rho_{30}, \delta_0) \\ &= \mathcal{E} - TS - \sum_{i=n,p,e} \mu_i n_i \end{aligned} \quad (6)$$

model	n_0 (fm $^{-3}$)	E_0 (MeV)	K_0 (MeV)	Q_0 (MeV)	E_{sym} (MeV)	L (MeV)
NL3	0.148	-16.24	270.7	203	37.3	118.3
TM1	0.145	-16.26	280.4	-295	36.8	110.6
FSU	0.148	-16.30	230.0	-523	32.6	60.5
NL3 $_{\omega\rho}$	0.148	-16.30	272.0	203	31.7	55.2
DD-ME δ	0.152	-16.12	219.1	-741	32.4	52.9
DD-ME2	0.152	-16.14	250.8	478	32.3	51.4
IU-FSU	0.155	-16.40	231.2	-288	31.3	47.2

TABLE I: Nuclear matter properties at saturation: density (n_0), energy (E_0), incompressibility (K_0), skewness (Q_0), symmetry energy (E_{sym}), and symmetry energy slope parameter (L).

where $\{f_{i+}\}(\{f_{i-}\})$ with $i = n, p, e$ stands for the neutron, proton and electron positive (negative) energy distributions, and \mathcal{S} and \mathcal{E} are the total entropy and energy densities, respectively [9]. The equations of motion for the meson fields (see *e.g.*, Ref. [7] for details) follow from the variational conditions

$$\frac{\delta \Omega}{\delta \sigma(\mathbf{r})} = \frac{\delta \Omega}{\delta \omega_0(\mathbf{r})} = \frac{\delta \Omega}{\delta \rho_{30}(\mathbf{r})} = \frac{\delta \Omega}{\delta \delta_0(\mathbf{r})} = 0, \quad (7)$$

where $\Omega = \int d^3r \omega$. The numerical algorithm for the description of the neutral npe matter at finite temperature is a generalization of the $T = 0$ case which is discussed in detail in Refs. [7, 9]. The Poisson equation is always solved by using the appropriate Green's function according to the spatial dimension of interest, and the Klein-Gordon equations are solved by expanding the meson fields in a harmonic oscillator basis with one, two or three dimensions based on the method presented in Refs. [7, 9]. The interested reader is referred to these works for details of the calculation.

III. RESULTS

In this section we present and discuss the results obtained for the different models considered. The section is divided in three parts. In the first one our attention is focused on the sensitivity of the thickness and structure of the inner crust to the properties of the EoS. In the second one we discuss the effect of L on the density profile of the crust. Finally, in the last part we analyze the effect of finite temperature on the crust and the pasta phase. The discussion is done for neutron stars with masses $M = 1, 1.44$ and $1.6M_\odot$. The first two values have been chosen as representative masses since $1M_\odot$ is smaller than the smallest neutron star mass detected until now and $1.44M_\odot$ is the mass of the famous Hulse-Taylor pulsar. The value of $1.6M_\odot$ is chosen to be slightly smaller than the maximum mass predicted by the FSU model. Results for the maximum neutron star mass configuration have also been obtained for all the models.

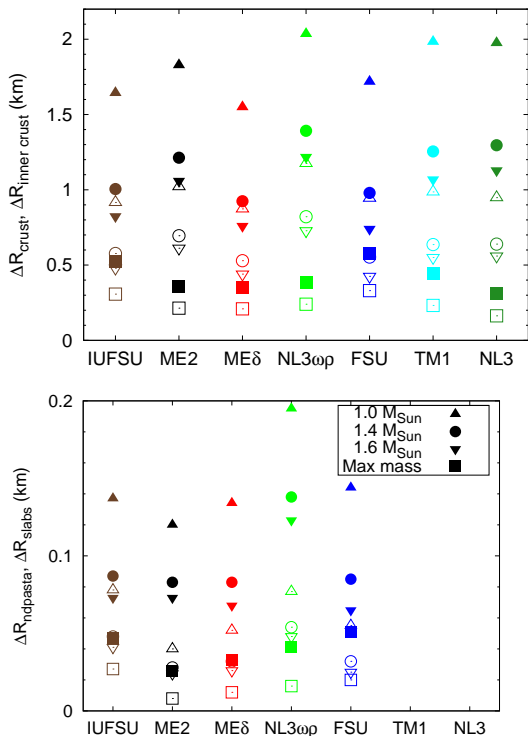


FIG. 1: (Color online) Top panel: Crust (full symbols) and inner crust (empty symbols) thickness. Bottom panel: Thickness of the non-droplet pasta (ndpasta) (full symbols) and the slab (empty symbols) phases. The symbol shape identifies the star mass: 1.0 M_{\odot} (upward triangle), 1.44 M_{\odot} (circle), 1.6 M_{\odot} (downward triangle) and maximum mass (square).

A. Thickness and structure of the inner crust

We present here results for the pasta phase of β -equilibrium non-homogeneous matter obtained within our TF calculation at $T = 0$. As done by many authors, we assume that for some given conditions (temperature, density, proton fraction or chemical equilibrium) only a single geometry will be the physical one, *i.e.*, the one with smaller free energy in comparison with homogeneous β -stable matter. At least five different geometries could in principle occur: droplets, rods, slabs, tubes and bubbles. However, due to the β -equilibrium the proton fraction is very small and only three of them are found energetically favorable: droplets, rods and slabs. These structures form a regular lattice that we study in the WS approximation. The TF approach is semiclassical and does not include shell effects. Nevertheless, it has been recently shown [12] that the main properties of the WS cells obtained within a TF calculation agree with Hartree–Fock (HF) [32] and Hartree–Fock–Bogoliubov (HFB) [33] calculations which allow the inclusion of shell effects. For a comparison of HFB and TF results the interested reader is referred to Ref. [12].

The complete stellar matter EoS is built by properly joining the inner crust part with the outer crust and the

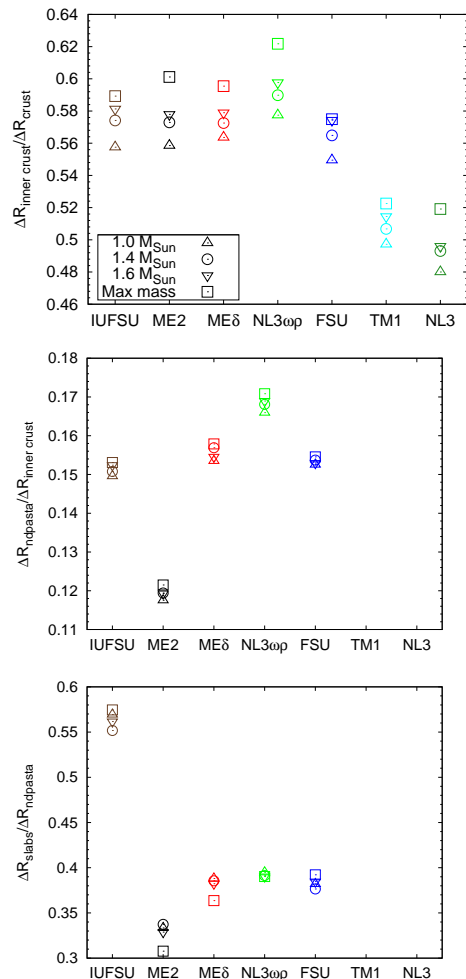


FIG. 2: (Color online) Top panel: Fraction of the crust occupied by the inner crust. Middle panel: Fraction of the inner crust occupied by the non-droplet pasta (ndpasta) phase. Bottom panel: Fraction of the non-droplet pasta phase occupied by the slab phase. The symbol shape has the same meaning as in Fig. 1.

core ones. In this work, we assume that the core of the star is made only of nucleons, electrons and muons, and its EoS is obtained also in RMF approach imposing both β -equilibrium and charge neutrality. For the outer crust we consider the well known Baym–Pethick–Sutherland (BPS) EoS [31]. The TOV equations are then solved to determine the density profile of the neutron stars with the masses $M = 1, 1.44, 1.6 M_{\odot}$ and M_{max} mentioned before.

In Table II we show for the different models some of the features of the inner crust structure. All the models have a slab and a rod phase which together define the thickness of the non-droplet pasta, except for the NL3 and TM1 models. For these two models the inner crust is only formed by droplets in a neutron gas background. This is, as shown in Ref. [11], due to the high value of L for these two models, 118 MeV and 110 MeV, respectively.

In order to help the discussion, the results of Table II

are also plotted, in Figs. 1 and 2. In Fig. 1, the thickness of the total crust (full symbols) and inner crust (empty symbols) are shown in the top panel, and the thickness of the total non-droplet pasta phase (full symbols) and the slab phase (empty symbols) are plotted in the bottom panel. In Fig. 2 we plot the ratios of these quantities: the fraction of the inner crust with respect to the total crust (top panel), the fraction of the non-droplet pasta extension with respect to the total inner crust (middle panel) and the fraction of slab phase size with respect to the total non-droplet phase (bottom panel). The different models are ordered according to the magnitude of the slope L , which increases from left to right.

From Fig. 1 we see that no clear trend is found in the thickness of the different parts as a function of L . Instead, we have found (see Fig. 3) that the size of the total crust is mainly defined by the incompressibility of the EoS (cfr Table I). In particular, the models NL3, NL3 $\omega\rho$, TM1, followed by DDME2, have the largest crusts and the largest incompressibilities. In general, a systematic behaviour is observed with the mass of the star: the larger the mass, the thinner the crust and its sub-layers. For instance, in all cases for $M = 1 M_\odot$ the crust thickness lies between 1.5 and 2 km, while for the maximum mass configurations it is mainly below 0.5 km.

The top panel of Fig. 2 shows that the inner crust occupies $\gtrsim 55\%$ of the total crust size, except for NL3 and TM1, for which it reduces to $\sim 50\%$ of it. Once more, a systematic dependence upon the star mass is found: the fraction of the crust occupied by the inner crust increases with the star mass and there is a difference of $\sim +2\%$ between a star with 1 and 1.6 M_\odot .

Next, we come to the size of the non-droplet pasta phase, the phases that correspond to a frustrated system. In a 1 M_\odot star the non-droplet pasta size is smaller than 200 m (Fig. 1 bottom). Its relative size is slightly smaller in less massive stars (Fig. 2 middle). Within the non-droplet pasta phase, we find in our results slabs and rods phases. The slab fraction corresponds to $\sim 35-40\%$ of the total non-droplet pasta phase for all the models, apart from IU-FSU, where it is almost 60% and DDME2 with $\sim 30-35\%$ (Fig. 2 bottom). The different behavior of IU-FSU is mainly due to the small proton fraction in the cluster. IU-FSU has a small value of the symmetry energy slope at subsaturation densities, which affects the surface tension giving quite a high surface tension, see [12], and preventing the neutron drip. A small proton fraction in the cluster favors the slab geometry with respect to the rod geometry because the surface energy decreases with the proton fraction. On the contrary, a smaller surface tension favors the neutron drip. Clusters are more isospin symmetric and the droplet geometry is favored. This could explain the behavior of DDME2 with the smallest fraction of the non-droplet pasta phase. In Ref. [12] it is shown that the DDME2 and NL3 models have the smallest surface energies for nuclear symmetric matter.

In Ref. [37] the effect of the nuclear pasta on the crustal

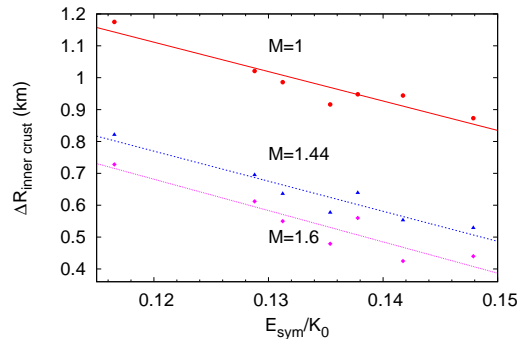


FIG. 3: (Color online) Correlation between the inner crust thickness and the ratio E_{sym}/K_0 for star with $M = 1, 1.44, 1.6 M_\odot$. The slope of the three straight lines is similar $\sim -9.5 \pm 15\%$ km.

shear phenomena was studied. In particular, two limits were considered, namely the pasta as an elastic solid and as a liquid. In the first case the shear modulus was calculated at the crust-core transition while in the second case it was done at the transition from the droplet phase to the non-droplet pasta phase. For models with no non-droplet pasta phase, such as NL3 and TM1, there is no difference between these two pictures. However, models with a symmetry energy slope L below 80 MeV, have a non-droplet pasta phase, and the ratio shear modulus to pressure can be as high as two times larger if the pasta is considered an elastic solid and $L = 40$ MeV. An intermediate picture would consider the rod phase as an elastic solid and the slab phase as a liquid phase.

Comparing our results with the ones discussed in [37] a couple of comments are in order. First, the incompressibility of the EoS seems to have an important influence on the total crust, so that DDME2 with $L = 51$ MeV has a larger crust than FSU with $L = 60$ MeV. Second, except for NL3 $\omega\rho$ with a large K_0 , all the other models predict the non-droplet pasta phase of the 1.44 M_\odot star with a thickness of ~ 80 m, similar to the one calculated in [37].

As mentioned before both the incompressibility and the density dependence of the symmetry energy affect the size of the inner crust. We have obtained a possible correlation between the ratio E_{sym}/K_0 and the inner crust thickness. This correlation is shown in Fig. 3. This should be further investigated and confirmed with a larger set of models. The correlation is worse for the 1.6 M_\odot star, probably because this mass lies closer to the maximum mass configuration. The slope obtained for the three star masses analysed is $\sim -9.5 \pm 15\%$ Km.

B. Density profile of the crust

In Fig. 4 we present the profile of stars with masses $M = 1, 1.44, 1, 60 M_\odot$ and M_{max} . The whole star profile

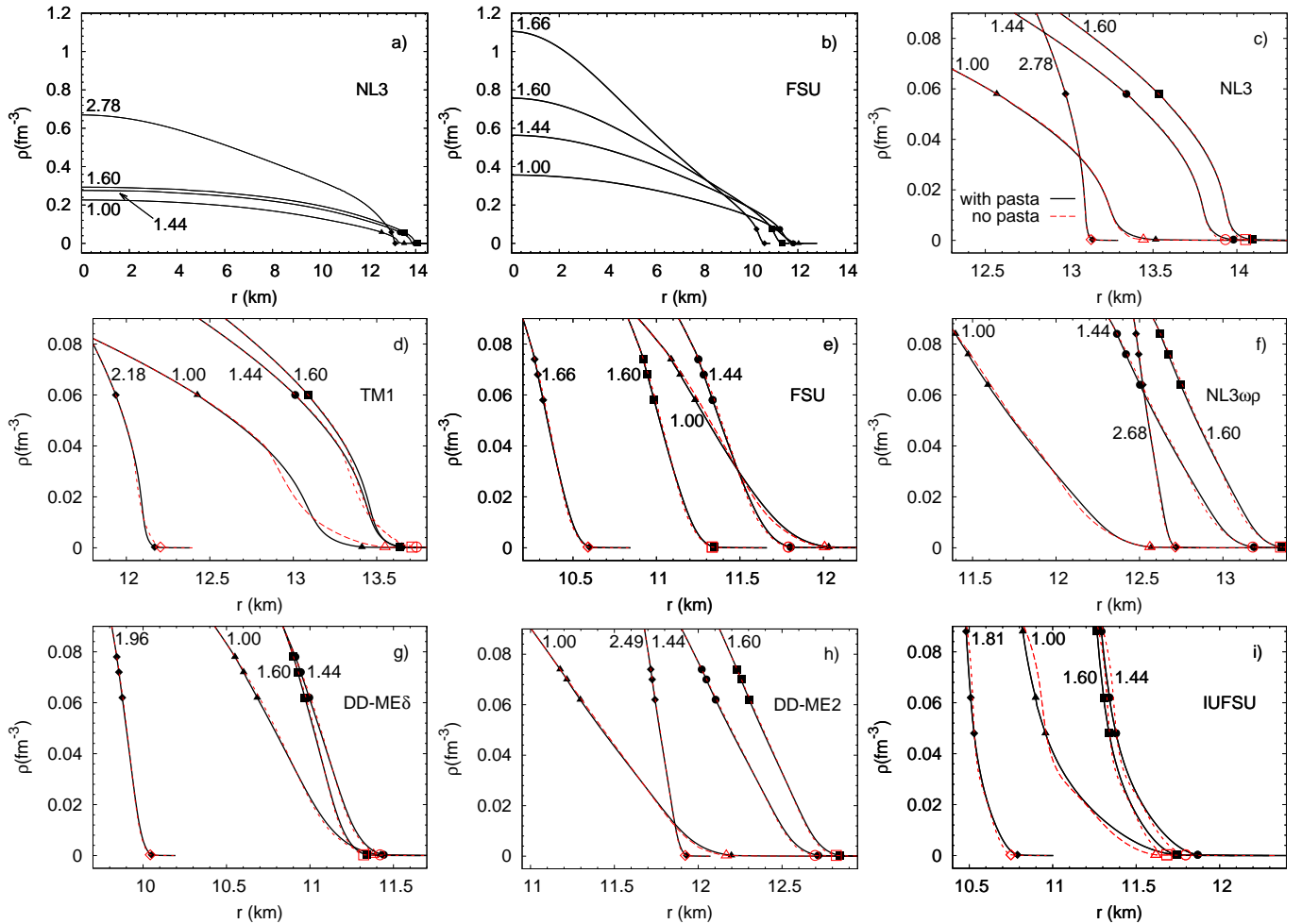


FIG. 4: (Color online) Profiles of neutron stars with a mass equal to $1.0 M_{\odot}$, $1.44 M_{\odot}$, $1.6 M_{\odot}$ and the maximum mass, for different nuclear models. The symbols stay at the the BPS-droplet, droplet-rod, rod-slab, slab-homogeneous transition for $1.0 M_{\odot}$ (triangle), $1.44 M_{\odot}$ (circle), $1.6 M_{\odot}$ (square) and maximum mass (diamond). Figures a) and b) show the complete profile for NL3 and FSU, respectively. All other panels [c) to i)] focus on the crust profile.

is shown for the models NL3 and FSU in Figs. 4a and 4b, respectively, since these two models predict the largest and the smallest maximum mass configuration.

All the other panels of Fig. 4 show, instead, for the whole set of models under discussion, only the last ~ 2 km of the star profile close to the surface. The results determined with the same EoS presented in the previous section (*i.e.*, including the TF calculation of the inner crust) are represented by a solid black line, and the transitions between the different phases of the inner crust are identified with black full symbols. For comparison, it is also shown the result obtained joining the BPS EoS directly to the homogeneous stellar matter EoS (red dashed lines). In this case, the transition from the BPS to the homogeneous matter is shown by a red empty symbol. The EoSs of the inner crust obtained within the TF framework and used to calculate the crust profiles are given in Tables IV and V of the Appendix.

Within the same model, a larger mass corresponds to a steeper profile, as expected, due to the larger gravi-

tational force. In models with a large incompressibility, like NL3, TM1, NL3 $\omega\rho$ and DDME2, and taking only the 1, 1.44 and $1.6 M_{\odot}$ stars, the star with the largest mass has the inner crust at a larger distance from the center. On the contrary, in the case of FSU, IU-FSU and DDME δ there is a larger concentration of mass at the center because the EoS is softer, and the crust is pushed more strongly towards the center of the star: this explains why for IU-FSU and DDME δ the profiles of the 1.44 and $1.6 M_{\odot}$ stars are almost coincident, and for FSU the profiles of the 1.0 and $1.44 M_{\odot}$ stars cross, while the crust of the $1.6 M_{\odot}$ one has the smallest distance to the star center. Notice that for NL3, TM1, and DDME2 also the maximum mass star has the smallest radius.

One interesting conclusion is that taking into account the correct description of the inner crust in the total stellar EoS is more important for the softer EoS and with smaller slopes L . However, on the whole, using the BPS EoS for the outer crust and an EoS of homogeneous stellar matter for the inner crust and core gives good results

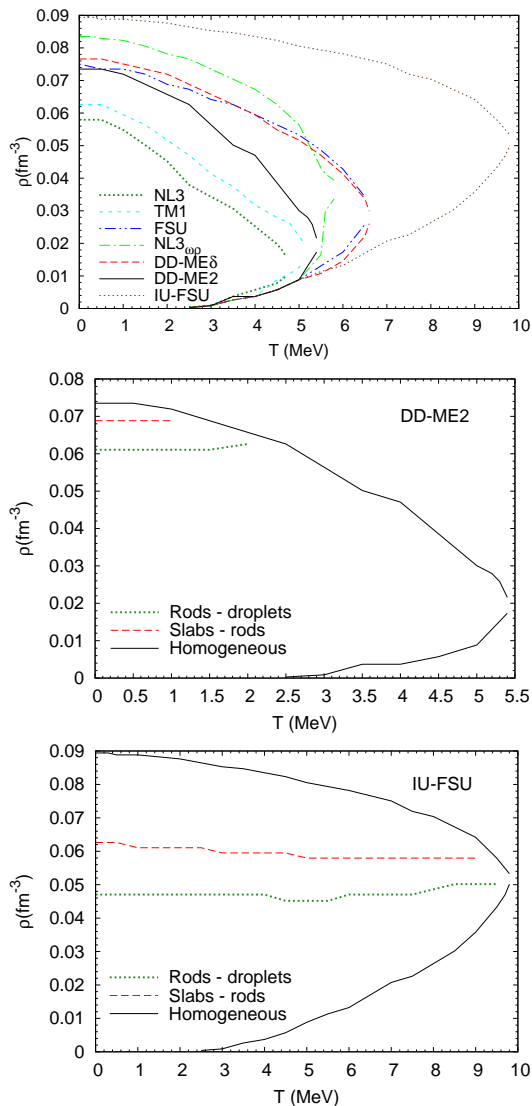


FIG. 5: (Color online) Top panel: density range of the crust as a function of temperature for all the models considered in the present study (top panel). Middle and bottom: size of the pasta phases versus T for DDME2 and IU-FSU. In these two panels, the dotted (dashed) line represents the transition droplet-rod (rod-slab).

for the stellar profiles.

C. Finite temperature effects on the crust

In this section we present the results of a finite temperature calculation of the crust size for β -equilibrium matter. Our main objectives are: i) to determine the critical temperatures below which clusterization should be taken into account; ii) to verify how temperature affects the pasta phase, particularly the transition between the different geometries and the size of the cells; and iii) to determine the melting temperature of clusters with

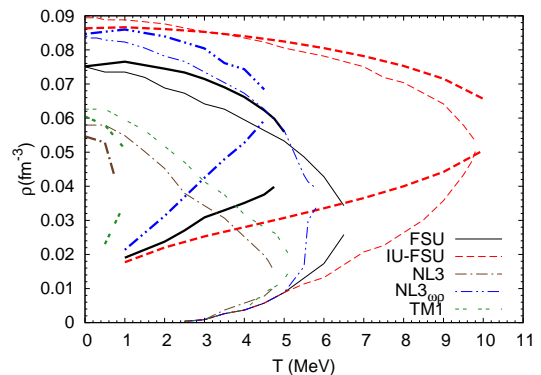


FIG. 6: (Color online) Density range of the crust as a function of temperature for some of the relativistic mean field models considered in the present study (top panel), using a TF calculation (thin lines) and a DS calculation (thick lines).

different geometry.

We perform the study using both a finite temperature TF calculation of the pasta phase and the finite temperature dynamical approach within the relativistic Vlasov formalism [16–18]. In the latter case, the crust-core transition is defined by the intersection between the β -equilibrium EoS and the dynamical spinodal (DS); The cluster size is identified with half the wavelength of the density fluctuation [16, 17, 19]. The results are shown in Fig. 5 for the TF calculation; a comparison between the TF and the DS calculation is done in Fig. 6 and in Table III.

The critical temperature is model dependent and both the density dependence of the symmetry energy and the incompressibility affect this quantity: a smaller value of L and a smaller K_0 favor clusterization at larger temperatures. The results obtained within the TF approach are compatible with the estimations calculated using the dynamical calculation at the bottom of the inner crust. Close to the outer crust the dynamical calculations estimations give much larger densities. This could be expected, considering that in the TF calculation the inner crust in this region is formed by small droplets inside cells with a much larger radius. On the other hand, the dynamical calculation considers always that the cluster size is half the WS cell, and therefore, has a much larger surface energy contribution. Our results are compatible with the ones obtained in Ref. [19] (see Fig. 11 of this reference), where most of the results have been obtained for Skyrme forces.

From the middle and lower panels of Fig. 5, we observe that the droplet-rod and the rod-slab transition densities do not depend on the temperature. However, the melting temperature of the three geometries is different, with the droplets surviving up to higher temperatures.

In the present calculation we suppose that the WS cells exist until the clusters melt. This is an approximation that will probably break down close to the melting point due to thermal fluctuations, and therefore, the numbers

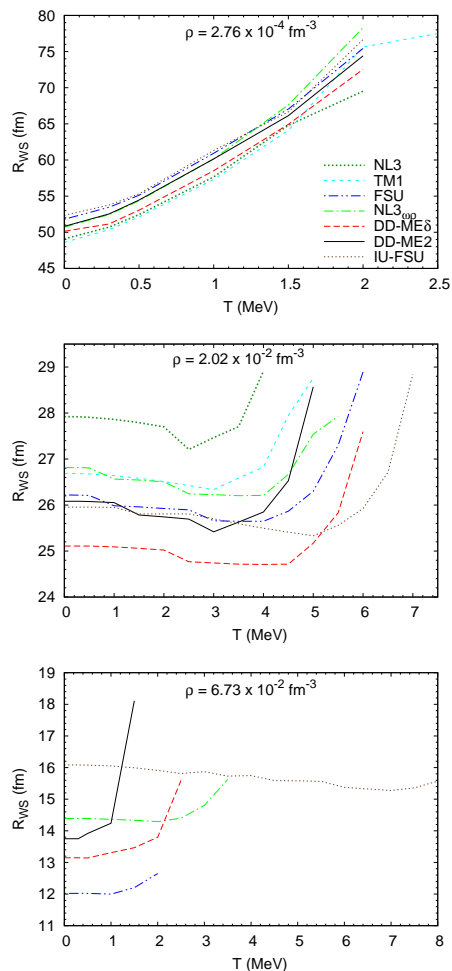


FIG. 7: (Color online) Radius of the cells as a function of the temperature at the densities reported in top of the figures.

obtained should be interpreted as an upper limit. The problem of the effect of thermal fluctuations on the pasta structures has been studied in Refs. [20, 21] and it has been shown that thermally induced displacements of the rodlike and slablike nuclei can melt the lattice structure when these displacements are larger than the space available between the cluster and the boundary of the WS cell. Moreover, it was also shown that slablike nuclei would more easily be dissolved, while the rodlike were expected to survive at temperatures relevant for supernova cores. In the present calculation, except for IU-FSU, all models predict the melting of the slabs at a temperature $T < 3$ MeV, while the rods will melt at temperatures one MeV higher, see Table III. Neglecting thermal fluctuations we expect that clusters will survive in β -equilibrium matter at temperatures below 5 – 6 MeV, approximately twice the melting temperature of non-droplet structures.

We next analyse the effect of the temperature on the size of the WS cells. In Fig. 7 we plot the WS radius as a function of the temperature for all the models. We select three reference densities: $\rho = 2.76 \times 10^{-4}$ and 2.02

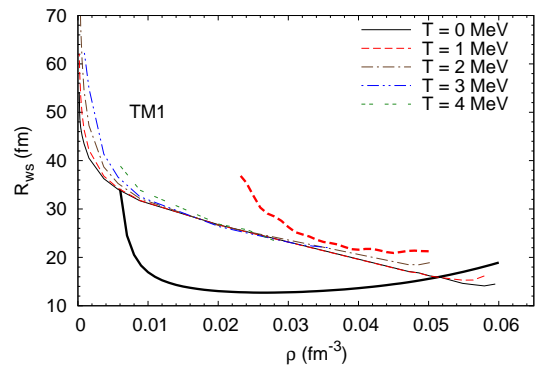


FIG. 8: (Color online) Radius of the cells as a function of the matter density for the TM1 model within the DS calculation (thick lines) and TF calculation (thin lines).

$\times 10^{-2} \text{ fm}^{-3}$, at which the clusters are spherical for all models, and $\rho = 6.73 \times 10^{-2} \text{ fm}^{-3}$, where all are in rod phase except IU-FSU, that is in a slab phase. In Fig. 8 we focus on the TM1 model, which only shows spherical clusters, and plot the radius of the WS cell versus density at different temperatures.

In general, for the densities shown, the WS radius increases with the temperature, but for $\rho = 2.02 \times 10^{-2} \text{ fm}^{-3}$ the R_{WS} suffers a small decrease of the order of 0.5 fm below $T = 3 - 4$ MeV. The surface energy decreases with temperature, and, as a result, we could expect that the Wigner Seitz radius would decrease with temperature. This, in fact, occurs for temperatures well below the critical transition temperature to homogeneous matter, corresponding to the behavior below $T \lesssim 4$ MeV in the Fig. 7 middle panel for most of the models considered, or to the IUFSU below 7 MeV and NL3 $\omega\rho$ below 2 MeV in the bottom figure. However, for temperatures close to the critical temperature, the Wigner Seitz radius increases most probably due to the restrictions of the present calculation which does not allow the freedom for the cluster to choose the shape that minimizes the free energy. A similar behavior was obtained within a different formalism, namely considering plane-wave density fluctuations and relating the wave number of the unstable modes with the Wigner Seitz cell size. In [19] and [18], both in the framework of the non-relativistic Skyrme interactions and the RMF nuclear models, the Wigner Seitz cell increases with the temperature. In this case the size of the Wigner Seitz cell is identified with the wave-length of the perturbation, and the cluster size with half-wave length, and the system does not have the freedom to have the size of the cluster and of the cell uncorrelated.

We have performed a calculation of the WS radius within a DS calculation for TM1 and $T = 0$, and 1 MeV (thick lines in Fig. 8). TF and DS give similar sizes for $T = 0$ MeV at the bottom of the inner crust, where the dynamical calculation predicts non-homogeneous matter. However, in general the DS predictions are quite different from the TF results, in particular quite smaller at $T = 0$

MeV and larger at finite T .

IV. CONCLUSIONS

In the present work the inner crust, including the non-spherical pasta phases, was calculated within a self-consistent Thomas–Fermi approach [7, 8] for β -equilibrium matter at zero and finite temperature. Several relativistic nuclear models, both with constant and density dependent couplings, have been considered.

All models, except NL3 and TM1, both with a symmetry energy slope at saturation above 110 MeV, predict the existence of *lasagna*-like structures that may have an important contribution to the specific heat of the crust [36].

The effect of the inner crust EoS on the neutron star profiles was also analysed. It was verified that a smaller slope gives rise to a steeper crust density profile and a larger inner crust with respect to the total crust. It may also enhance the slab phase size as observed in IU-FSU.

It was observed that the star profile obtained using the TF inner crust calculation or the homogeneous EoS above the outer-inner crust transition did not differ much except for the models with a large symmetry energy slope.

The finite temperature calculation of the pasta phase in β -equilibrium has shown that non-homogeneous matter is expected for temperatures below 5-6 MeV, the only exception was obtained with the parametrization IU-FSU which only melts at 9.5 MeV. Non-spherical structures, rodlike and slablike, melt above, respectively, 2-3.5 MeV and 1-3 MeV. It was also verified that the onset density of the rodlike and the slablike structures is independent of the temperature.

Finally, it was shown that a DS calculation is able to give a good prediction of the crust-core transition, even at finite temperature. However, considering the size of the WS cells, this formalism fails except for $T = 0$ MeV close to the crust-core transition.

Acknowledgments

We are grateful to Silvia Chiacchiera for the careful reading of the manuscript and for the editing of the figures. This work has been partially supported by QREN/FEDER, the Programme COMPETE, and FCT (Portugal) under the projects PTDC/FIS/113292/2009 and CERN/FP/123608/2011, by the Capes/FCT n. 232/09 bilateral collaboration.

-
- [1] D. G. Ravenhall, C. J. Pethick, and J. R. Wilson, Phys. Rev. Lett. **50**, 2066 (1983).
- [2] M. Hashimoto, H. Seki, and M. Yamada, Prog. Theor. Phys. **71**, 320 (1984).
- [3] C. J. Horowitz, M. A. Pérez-García, and J. Piekarewicz, Phys. Rev. C **69**, 045804 (2004); C. J. Horowitz, M. A. Pérez-García, D. K. Berry, and J. Piekarewicz, *ibid.* **72**, 035801 (2005).
- [4] G. Watanabe, K. Sato, K. Yasuoka, and T. Ebisuzaki, Phys. Rev. C **66**, 012801 (2002); **68**, 035806 (2003); **69**, 055805 (2004); H. Sonoda, G. Watanabe, K. Sato, K. Yasuoka, and T. Ebisuzaki, *ibid.* **77**, 035806 (2008).
- [5] F. Douchin, and P. Haensel, A&A **380**, 157 (2001).
- [6] T. Maruyama, T. Tatsumi, D.N. Voskresensky, T. Tanigawa and S. Chiba, Phys. Rev. C **72**, 015802 (2005).
- [7] S. S. Avancini, D. P. Menezes, M. D. Alloy, J. R. Marinelli, M. M. W. de Moraes and C. Providência, Phys. Rev. C **78**, 015802 (2008).
- [8] S. S. Avancini, L. Brito, J. R. Marinelli, D. P. Menezes, M. M. W. de Moraes, C. Providência, and A. M. Santos, Phys. Rev. C **79**, 035804 (2009).
- [9] S. S. Avancini, S. Chiacchiera, D. P. Menezes, and C. Providência, Phys. Rev. C **82**, 055807 (2010); Phys. Rev. C **85**, 059904(E) (2012).
- [10] H. Pais and J. R. Stone Phys. Rev. Lett. **109**, 151101 (2012).
- [11] K. Oyamatsu and K. Iida, Phys. Rev. C **75**, 015801 (2007).
- [12] F. Grill, C. Providência and S. S. Avancini, Phys. Rev. C **85**, 055808 (2012).
- [13] S. S. Avancini, C. C. Barros, Jr., L. Brito, S. Chiacchiera, D. P. Menezes, and C. Providência Phys. Rev. C **85**, 035806 (2012).
- [14] C. Providência *et al*, arXiv:1307.1436 [nucl-th].
- [15] J. R. Oppenheimer and G. M. Volkoff, Phys. Rev. **55**, 374 (1939); R. C. Tolman, *ibid.* **55**, 364 (1939).
- [16] C. Providência, L. Brito, S. S. Avancini, D. P. Menezes, and Ph. Chomaz Phys. Rev. C **73**, 025805 (2006).
- [17] L. Brito, C. Providência, A. M. Santos, S. S. Avancini, D. P. Menezes, and Ph. Chomaz Phys. Rev. C **74**, 045801 (2006).
- [18] H. Pais, A. Santos, L. Brito, and C. Providência Phys. Rev. C **82**, 025801 (2010); H. Pais, A. Santos, and C. Providência Phys. Rev. C **80**, 045808 (2009).
- [19] C. Ducoin, C. Providência, A. M. Santos, L. Brito and Ph. Chomaz, Phys. Rev. C **78**, 055801 (2008).
- [20] C. J. Pethick and A. Y. Potekhin, Phys. Lett. B **427**, 7 (1998).
- [21] G. Watanabe, K. Iida, and K. Sato, Nucl. Phys. A **676**, 455 (2000); Nucl. Phys. A **687**, 512 (2001); **726**, 357 (2003);
- [22] J. Boguta and A. R. Bodmer, Nucl. Phys. A **292**, 413 (1977).
- [23] S. Typel and H. H. Wolter, Nucl. Phys. A **656**, 331 (1999).
- [24] G. A. Lalazissis, J. König, and P. Ring, Phys. Rev. C **55**, 540 (1997).
- [25] Y. Sugahara and H. Toki, Nucl. Phys. A **579**, 557 (1994).
- [26] C. J. Horowitz and J. Piekarewicz, Phys. Rev. Lett. **86**, 5647 (2001); C. J. Horowitz and J. Piekarewicz, Phys. Rev. C **64**, 062802 (2001).
- [27] B. G. Todd-Rutel and J. Piekarewicz, Phys. Rev. Lett. **95**, 122501 (2005).
- [28] F. J. Fattoyev, C. J. Horowitz, J. Piekarewicz, and G.

- Shen, Phys. Rev. C **82**, 055803 (2010).
- [29] G. A. Lalazissis, T. Niksić, D. Vretenar, and P. Ring, Phys. Rev. C **71**, 024312 (2005).
- [30] X. Roca-Maza, X. Viñas, M. Centelles, P. Ring, and P. Schuck, Phys. Rev. C **84**, 054309 (2011).
- [31] G. Baym, C. Pethick, and P. Sutherland, Astrophys. J. **134**, 683 (1971).
- [32] J. N. Negele, and D. Vautherin, Nucl. Phys. A **207**, 298 (1973).
- [33] F. Grill, J. Margueron, and N. Sandulescu, Phys. Rev. C **84**, 065801 (2011).
- [34] I. Vidaña, C. Providência, A. Polls, and A. Rios Phys. Rev. C **80**, 045806 (2008).
- [35] C. Ducoin, J. Margueron, and C. Providência, Europhys. Lett. **91**, 32001 (2010)); C. Ducoin, J. Margueron, C. Providência and I. Vidaña, Phys. Rev. C **83**, 045810 (2011).
- [36] L. Di Gallo, M. Oertel, and M. Urban, Phys. Rev. C **84**, 045801 (2011).
- [37] M. Gearheart, W. G. Newton, J. Hooker, and Bao-An Li, MNRAS **418**, 2343 (2011).

Appendix: Equation of state of the inner crust

M (M_\odot)	ρ_c (fm^{-3})	\mathcal{E}_c (fm^{-4})	R_{h-s} (km)	R_{s-r} (km)	R_{r-d} (km)	R_{d-BPS} (km)	R (km)
NL3							
1.00	0.226	1.121	12.568*	-	-	13.516	14.543
1.44	0.276	1.390	13.341*	-	-	13.980	14.637
1.60	0.293	1.489	13.534*	-	-	14.094	14.663
2.78	0.669	4.415	12.978*	-	-	13.141	13.292
TM1							
1.00	0.243	1.208	12.425*	-	-	13.411	14.408
1.44	0.328	1.674	13.012*	-	-	13.648	14.267
1.60	0.366	1.893	13.089*	-	-	13.639	14.158
2.18	0.851	5.345	11.937*	-	-	12.169	12.381
FSU							
1.00	0.356	1.814	11.088	11.143	11.232	12.032	12.806
1.44	0.564	3.073	11.251	11.283	11.336	11.804	12.230
1.60	0.757	4.394	10.921	10.946	10.986	11.346	11.661
1.66	1.105	7.100	10.270	10.290	10.321	10.600	10.844
NL3 $_{\omega\rho}$							
1.00	0.256	1.277	11.397	11.474	11.592	12.572	13.432
1.44	0.298	1.518	12.365	12.419	12.503	13.186	13.757
1.60	0.314	1.616	12.624	12.672	12.747	13.352	13.842
2.68	0.680	4.640	12.479	12.495	12.520	12.719	12.865
DD-ME δ							
1.00	0.405	2.040	10.550	10.602	10.684	11.423	12.099
1.44	0.552	2.890	10.913	10.945	10.996	11.442	11.837
1.60	0.627	3.360	10.901	10.927	10.969	11.341	11.661
1.96	1.214	7.938	9.843	9.855	9.876	10.052	10.194
DD-ME2							
1.00	0.289	1.435	11.177	11.217	11.297	12.198	13.005
1.44	0.347	1.755	12.021	12.049	12.104	12.716	13.234
1.60	0.371	1.895	12.232	12.256	12.305	12.844	13.291
2.49	0.817	5.345	11.717	11.725	11.743	11.931	12.073
IU-FSU							
1.00	0.342	1.780	10.820	10.898	10.957	11.736	12.463
1.44	0.474	2.607	11.292	11.340	11.379	11.869	12.297
1.60	0.558	3.182	11.265	11.306	11.338	11.744	12.089
1.81	0.987	6.662	10.482	10.509	10.529	10.789	11.003

TABLE II: Central density (ρ_c) and energy density (\mathcal{E}_c), distance to the center of the star at the phase transitions: homogeneous matter–slab phase (R_{h-s}), slab phase–rod phase (R_{s-r}), rod phase–droplet phase (R_{r-d}), droplet phase–outer crust (R_{d-BPS}) and radius of a $1.0 M_\odot$, $1.44 M_\odot$, $1.6 M_\odot$ and maximum mass neutron star for the all the RMF models considered. For NL3 and TM1 there are neither slabs nor rods: the values marked with an asterisk correspond to the homogeneous matter–droplet phase transition.

model	ρ_{h-s}	ρ_{s-r}	ρ_{r-d}	T_s	T_r	T_m	
	(fm^{-3})	(fm^{-3})	(fm^{-3})	(MeV)	(MeV)	(MeV)	
	TF	DS					
NL3	0.0579	0.0546	-	-	-	4.7	
TM1	0.0626	0.0604	-	-	-	5.1	
FSU	0.0751	0.0751	0.0673	0.0580	2.5	3.5	6.5
NL3 $_{\omega\rho}$	0.0835	0.0846	0.0751	0.0642	3.0	3.5	5.8
DD-ME δ	0.0766	-	0.0720	0.0626	2.0	3.0	6.6
DD-ME2	0.0735	-	0.0688	0.0611	1.0	2.0	5.4
IU-FSU	0.0894	0.0863	0.0626	0.0471	9.0	9.5	9.8

TABLE III: Density transitions in the pasta phase at $T = 0$, and melting temperature of the different pasta phases. For the transition to uniform matter we also show the values obtained with a dynamical spinodal calculation (DS).

TABLE IV: Equation of state of the inner crust for the seven model considered. The energy density is given in unit of 10 fm^{-4} , while the pressure is in unit of 10^3 fm^{-4} .

$\rho \text{ (fm}^{-3}\text{)}$	NL3		TM1		FSU		NL3 $_{\omega\rho}$		DD-ME δ		DD-ME2		IU-FSU	
	\mathcal{E}	P	\mathcal{E}	P	\mathcal{E}	P	\mathcal{E}	P	\mathcal{E}	P	\mathcal{E}	P	\mathcal{E}	P
0.0860	-	-	-	-	-	-	-	-	-	-	-	-	4.13948	1.60166
0.0840	-	-	-	-	-	-	-	-	-	-	-	-	4.04284	1.57348
0.0820	-	-	-	-	-	-	3.94154	2.52403	-	-	-	-	3.94621	1.54348
0.0800	-	-	-	-	-	-	3.84480	2.41543	-	-	-	-	3.84959	1.50902
0.0780	-	-	-	-	-	-	3.74809	2.30744	-	-	-	-	3.75297	1.47400
0.0760	-	-	-	-	-	-	3.65141	2.20122	3.65126	2.04088	-	-	3.65637	1.43842
0.0740	-	-	-	-	-	-	3.55475	2.11172	3.55465	1.93136	-	-	3.55977	1.40239
0.0720	-	-	-	-	3.45832	1.86234	3.45812	2.01229	3.45807	1.82398	3.45856	2.06135	3.46319	1.36591
0.0700	-	-	-	-	3.36175	1.76038	3.36151	1.91484	3.36152	1.73271	3.36193	1.95675	3.36661	1.32916
0.0680	-	-	-	-	3.26521	1.66110	3.26494	1.81906	3.26500	1.63419	3.26533	1.86477	3.27005	1.29192
0.0660	-	-	-	-	3.16870	1.57890	3.16839	1.72541	3.16850	1.53902	3.16875	1.76524	3.17350	1.25411
0.0640	-	-	-	-	3.07221	1.48951	3.07187	1.63348	3.07203	1.44694	3.07221	1.66744	3.07696	1.21646
0.0620	-	-	-	-	2.97575	1.40336	2.97537	1.54804	2.97559	1.35825	2.97570	1.57160	2.98043	1.17734
0.0600	-	-	-	-	2.87932	1.31999	2.87891	1.46017	2.87918	1.27656	2.87922	1.48170	2.88391	1.15722
0.0580	-	-	2.77736	1.48251	2.78292	1.24043	2.78247	1.37452	2.78280	1.19477	2.78276	1.39043	2.78740	1.11951
0.0560	2.67959	1.36758	2.68110	1.33925	2.68654	1.16654	2.68607	1.29055	2.68644	1.11632	2.68634	1.30149	2.69090	1.08100
0.0540	2.58343	1.24190	2.58489	1.20460	2.59019	1.09281	2.58969	1.20876	2.59011	1.04117	2.58995	1.21468	2.59442	1.04177
0.0520	2.48731	1.10988	2.48873	1.07826	2.49387	1.02186	2.49334	1.12899	2.49381	0.96925	2.49359	1.13056	2.49795	1.00189
0.0500	2.39124	0.98623	2.39262	0.96135	2.39757	0.95359	2.39703	1.05140	2.39753	0.90079	2.39727	1.04932	2.40150	0.96104
0.0480	2.29522	0.87140	2.29656	0.85336	2.30130	0.88792	2.30074	0.97589	2.30129	0.83526	2.30097	0.97047	2.30506	0.91959
0.0460	2.19925	0.76548	2.20053	0.75398	2.20505	0.82493	2.20448	0.90271	2.20506	0.77288	2.20471	0.89456	2.20864	0.88260
0.0440	2.10332	0.66838	2.10455	0.66326	2.10884	0.76421	2.10826	0.83187	2.10887	0.71384	2.10848	0.82153	2.11224	0.83977
0.0420	2.00743	0.57990	2.00861	0.58036	2.01265	0.70583	2.01207	0.76345	2.01270	0.65749	2.01228	0.75175	2.01586	0.79629
0.0400	1.91158	0.49988	1.91270	0.50581	1.91648	0.65009	1.91591	0.69757	1.91656	0.60433	1.91612	0.68485	1.91950	0.75215
0.0380	1.81577	0.42802	1.81683	0.43892	1.82035	0.59632	1.81978	0.63438	1.82044	0.55375	1.81999	0.62125	1.82316	0.70710
0.0360	1.71999	0.36366	1.72099	0.37922	1.72424	0.54503	1.72368	0.57417	1.72435	0.50611	1.72389	0.56110	1.72684	0.66164
0.0340	1.62425	0.30710	1.62519	0.32641	1.62816	0.49573	1.62762	0.51660	1.62828	0.46111	1.62782	0.50414	1.63055	0.61573
0.0320	1.52854	0.25764	1.52941	0.27974	1.53211	0.44880	1.53159	0.46202	1.53224	0.41839	1.53179	0.45077	1.53429	0.56936
0.0300	1.43286	0.21487	1.43366	0.23935	1.43609	0.40395	1.43560	0.41054	1.43623	0.37826	1.43578	0.40065	1.43805	0.52279
0.0280	1.33721	0.17828	1.33793	0.20443	1.34009	0.36143	1.33963	0.36219	1.34024	0.34020	1.33981	0.35413	1.34185	0.47616
0.0260	1.24158	0.14742	1.24223	0.17453	1.24413	0.32094	1.24370	0.31724	1.24428	0.30452	1.24388	0.31080	1.24568	0.42990
0.0240	1.14597	0.12168	1.14655	0.14904	1.14819	0.28293	1.14781	0.27538	1.14835	0.27072	1.14797	0.27102	1.14955	0.38403
0.0220	1.05038	0.10070	1.05089	0.12750	1.05229	0.24695	1.05194	0.23687	1.05244	0.23894	1.05210	0.23433	1.05345	0.33888
0.0200	0.95481	0.08382	0.95525	0.10921	0.95642	0.21340	0.95611	0.20175	0.95656	0.20879	0.95625	0.20094	0.95740	0.29484
0.0180	0.85925	0.07034	0.85962	0.09385	0.86058	0.18198	0.86032	0.16967	0.86071	0.18046	0.86044	0.17033	0.86138	0.25222
0.0160	0.76371	0.05970	0.76401	0.08068	0.76478	0.15294	0.76455	0.14068	0.76489	0.15360	0.76467	0.14261	0.76542	0.21158
0.0140	0.66817	0.05118	0.66842	0.06917	0.66901	0.12598	0.66883	0.11489	0.66910	0.12837	0.66892	0.11747	0.66950	0.17301
0.0120	0.57265	0.04399	0.57284	0.05873	0.57327	0.10120	0.57313	0.09162	0.57335	0.10445	0.57321	0.09461	0.57364	0.13703

TABLE V: (Continuation).

ρ (fm ⁻³)	NL3		TM1		FSU		NL3 _{$\omega\rho$}		DD-ME δ		DD-ME2		IU-FSU	
	\mathcal{E}	P	\mathcal{E}	P	\mathcal{E}	P	\mathcal{E}	P	\mathcal{E}	P	\mathcal{E}	P	\mathcal{E}	P
0.0100	0.47714	0.03760	0.47697	0.04799	0.47758	0.07870	0.47748	0.07095	0.47764	0.08210	0.47754	0.07389	0.47783	0.10429
0.0095	0.45327	0.03608	0.45310	0.04561	0.45366	0.07338	0.45357	0.06618	0.45372	0.07673	0.45362	0.06897	0.45389	0.09659
0.0090	0.42939	0.03451	0.42923	0.04318	0.42975	0.06816	0.42966	0.06157	0.42980	0.07145	0.42971	0.06421	0.42995	0.08909
0.0085	0.40552	0.03289	0.40536	0.04074	0.40584	0.06309	0.40576	0.05706	0.40588	0.06624	0.40581	0.05955	0.40602	0.08184
0.0080	0.38165	0.03132	0.38149	0.03836	0.38193	0.05818	0.38186	0.05270	0.38197	0.06122	0.38190	0.05504	0.38209	0.07485
0.0075	0.35777	0.02970	0.35763	0.03588	0.35802	0.05336	0.35796	0.04840	0.35806	0.05620	0.35800	0.05058	0.35816	0.06806
0.0070	0.33390	0.02797	0.33376	0.03340	0.33412	0.04870	0.33407	0.04429	0.33415	0.05139	0.33410	0.04632	0.33424	0.06152
0.0065	0.31003	0.02630	0.30990	0.03096	0.31022	0.04414	0.31017	0.04024	0.31025	0.04657	0.31021	0.04211	0.31033	0.05529
0.0060	0.28617	0.02453	0.28604	0.02853	0.28633	0.03978	0.28629	0.03639	0.28635	0.04196	0.28631	0.03801	0.28642	0.04916
0.0055	0.26230	0.02270	0.26218	0.02605	0.26243	0.03552	0.26240	0.03264	0.26246	0.03750	0.26242	0.03406	0.26251	0.04338
0.0050	0.23843	0.02088	0.23832	0.02351	0.23855	0.03137	0.23852	0.02899	0.23856	0.03309	0.23854	0.03015	0.23861	0.03791
0.0045	0.21457	0.01895	0.21447	0.02108	0.21466	0.02742	0.21464	0.02544	0.21468	0.02889	0.21466	0.02645	0.21471	0.03269
0.0040	0.19071	0.01703	0.19061	0.01855	0.19078	0.02362	0.19076	0.02204	0.19079	0.02488	0.19078	0.02286	0.19082	0.02777
0.0035	0.16685	0.01500	0.16677	0.01606	0.16691	0.02002	0.16689	0.01880	0.16692	0.02098	0.16690	0.01941	0.16694	0.02316
0.0030	0.14299	0.01297	0.14292	0.01363	0.14304	0.01657	0.14303	0.01571	0.14304	0.01733	0.14304	0.01612	0.14306	0.01880
0.0025	0.11914	0.01095	0.11908	0.01125	0.11917	0.01333	0.11916	0.01272	0.11918	0.01389	0.11917	0.01297	0.11919	0.01485
0.0020	0.09529	0.00892	0.09524	0.00892	0.09532	0.01034	0.09531	0.00998	0.09532	0.01069	0.09531	0.01014	0.09533	0.01125
0.0015	0.07145	0.00694	0.07141	0.00674	0.07146	0.00755	0.07146	0.00745	0.07147	0.00780	0.07146	0.00745	0.07147	0.00806
0.0010	0.04761	0.00507	0.04759	0.00466	0.04762	0.00517	0.04762	0.00517	0.04762	0.00532	0.04762	0.00507	0.04763	0.00537
0.0009	0.04285	0.00466	0.04283	0.00431	0.04286	0.00476	0.04285	0.00476	0.04285	0.00487	0.04286	0.00466	0.04286	0.00487
0.0008	0.03808	0.00431	0.03806	0.00395	0.03809	0.00431	0.03809	0.00436	0.03809	0.00441	0.03809	0.00426	0.03809	0.00441
0.0007	0.03332	0.00395	0.03330	0.00360	0.03332	0.00395	0.03332	0.00400	0.03332	0.00400	0.03332	0.00385	0.03332	0.00400
0.0006	0.02855	0.00365	0.02854	0.00324	0.02856	0.00355	0.02855	0.00360	0.02856	0.00360	0.02856	0.00350	0.02856	0.00355
0.0005	0.02379	0.00334	0.02378	0.00289	0.02379	0.00314	0.02379	0.00324	0.02379	0.00324	0.02379	0.00314	0.02379	0.00319
0.0004	0.01902	0.00299	0.01902	0.00258	0.01903	0.00284	0.01903	0.00289	0.01903	0.00289	0.01903	0.00279	0.01903	0.00284
0.0003	0.01426	0.00258	0.01426	0.00228	0.01426	0.00248	0.01426	0.00253	0.01426	0.00253	0.01426	0.00243	0.01426	0.00248